Journal of Southeast University (English Edition) Vol. 38, No. 4, pp. 363 – 372 Dec. 2022 ISSN 1003—7985

Comparison of the vibration isolation performance of a seat suspension with various design modes

Zha Jili[1,2] Zhang Jianrun[3] Nguyen Van Liem[1,2]

([1]School of Mechanical and Electrical Engineering, Hubei Polytechnic University, Huangshi 435003, China)
([2]Hubei Key Laboratory of Intelligent Conveying Technology and Device, Hubei Polytechnic University, Huangshi 435003, China)
([3]School of Mechanical Engineering, Southeast University, Nanjing 211189, China)

Abstract: Three design modes of seat suspension, i.e., negative stiffness elements (NSEs), damping elements (DEs), and negative stiffness-damping elements (NSDEs), are proposed to evaluate the ride performance of a vehicle. Based on a dynamic model of a seat suspension and indexes of the root mean square deformation and acceleration of the seat suspension (x_{RMS}) and driver's seat (a_{RMS}), the influence of the design parameters of the NSEs, DEs, and NSDEs on the driver's ride comfort is evaluated. A genetic algorithm is then applied to optimize the parameters of the NSEs, DEs, and NSDEs. The study results indicate that the design parameters of the NSEs and NSDEs remarkably influence x_{RMS} and a_{RMS}, whereas those of the DEs insignificantly influence x_{RMS} and a_{RMS}. Based on the optimal results of the NSEs, DEs, and NSDEs, the damping force of the DEs is 98.3% lower than the restoring force of the NSEs. Therefore, the DEs are ineffective in decreasing x_{RMS} and a_{RMS}. Conversely, the NSEs combined with the damping coefficient of the seat suspension strongly reduce x_{RMS} and a_{RMS}. Consequently, the NSEs can be added to the seat suspension, and the damping coefficient of the seat suspension can also be optimized or controlled to further enhance the vehicle's ride performance.

Key words: seat suspension; negative stiffness elements; damping elements; ride performance; genetic algorithm
DOI: 10.3969/j.issn.1003 – 7985.2022.04.005

To enhance drivers' ride comfort in vehicles, seat suspension systems used by an air spring[1] and a damper with its active damping coefficient[2] or the optimization design for a body mounting system of heavy vehicles were studied and applied[3]. Moreover, based on the genetic algorithm (GA) and cultural algorithm, some control methods combining the GA-fuzzy control[4], cultural algorithm-fuzzy control[5], and GA-fuzzy control-proportional-integral-derivative control[6] were applied for the semi-active suspension system of vehicles. Moreover, based on the control rules of the fuzzy control controlled by the GA, the machine learning method[7] was investigated to further optimize the isolation performance of the seat suspension systems and ride comfort of vehicles. The results of the ride comfort were remarkably improved by semi-active suspension systems optimized and controlled by adaptive control methods. However, the isolation performance of the controlled seat suspension was only enhanced by up to 30% as compared to that of passive suspension systems, and the structure of the controlled suspension systems was quite complicated.

To solve the above issue, the negative stiffness element (NSE)[8–10], quasi-zero-stiffness[11], or magnetic negative stiffness damper[12] were proposed and researched to further reduce vibrations in the driver's seat. The influence of the geometrical dimension ratio and stiffness ratio of the NSE on the dimensionless characteristic of the restoring force-displacement and dynamic stiffness-displacement of the driver's seat was analyzed in detail to optimize the NSE's performance[13–14]. The different models of the NSE used by the curved-mount-spring-roller, air spring, and steel spring were investigated to assess the performance of the seat isolation system[9–10, 15–16]. The results show that the NSE added in the isolation system of the driver's seat not only greatly reduced the displacement and acceleration responses of the driver's seat but also significantly improved the power spectral density acceleration of the driver's seat in the low-frequency region. In addition, the optimal design of the NSE was proposed to further improve the isolation performance of the NSE[13–14]. However, in the existing research on the NSE for the driver's seat suspension systems, the influence of the NSE's design parameters was mainly analyzed via the dimensionless characteristic of the restoring force-displacement and dynamic stiffness-displacement[8, 16] and the driver's seat displacement and its root mean square (RMS) value[17]. The isolation performance of seat suspension systems should be evaluated via their deformation and the acceleration of the driver's seat rather than by the driver's seat displacement[1, 6, 18]. Moreover, with the seat suspension systems added by the NSE, its horizontal and

Received 2022-03-03, **Revised** 2022-07-10.

Biographies: Zha Jili (1980—), male, doctor; Zhang Jianrun (corresponding author), male, doctor, professor, zhangjr@seu.edu.cn.

Foundation items: The National Key Research and Development Plan (No. 2019YFB2006402), the Talent Introduction Fund Project of Hubei Polytechnic University (No. 19XJK20R), the Key Scientific Research Project of Hubei Polytechnic University (No. 22xjz02A).

Citation: Zha Jili, Zhang Jianrun, Nguyen Van Liem. Comparison of the vibration isolation performance of a seat suspension with various design modes[J]. Journal of Southeast University (English Edition), 2022, 38(4): 363 – 372. DOI: 10.3969/j.issn.1003 – 7985.2022.04.005.

symmetrical springs were used to generate the dynamic quasi-zero-stiffness and reduce the vibration of the seat suspension systems[9-10, 15-16]. Generally, a damper should be added to the suspension systems of vehicles, cabs, or seats to extinguish vibrations. Assuming that the stiffness element in the NSE is substituted using the damping element (DE) of the dampers or negative stiffness-damping element (NSDE), can the efficiency of the DE or NSDE be better than that of the NSE? Thus far, these issues have not been concerned and researched in the existing studies yet.

To clarify the above issues, a driver's seat dynamic model built under random excitation and combined harmonic excitation was used to assess the isolation performance of the NSE, DE, and NSDE in improving the driver's rider comfort and seat suspension deformation. The sensitivity effect of the design parameters on the isolation performance of the NSE, DE, and NSDE was analyzed via the indexes of the weighted RMS of the seat suspension deformation (x_{RMS}) and driver's seat acceleration (a_{RMS}). The NSE, DE, and NSDE parameters were then optimized based on the multi-objective optimization method to fully reflect the performance of the NSE, DE, and NSDE. The reduction of the seat suspension deformation and the increase in the driver's ride comfort are the goals of this study.

1 Driver's Seat Suspension System Models

1.1 Driver's seat suspension models

In the traditional driver's seat suspension (TDSS) of vehicles, the driver's seat suspension was mainly designed using dampers and springs[1-2, 4-5]. However, the TDSS's performance in reducing the driver's seat vibration is low. Thus, three various models of the TDSS added by the NSE, DE, and NSDE are proposed to evaluate their performance in ameliorating the driver's rider quality. Three various models of the TDSS are described as follows.

1.1.1 Model of the NSE added in the TDSS

The NSE is designed by two horizontal springs with the stiffness parameter k_s. It is installed horizontally and symmetrically at the TDSS position on the vehicle floor. One end of the horizontal spring is attached to a sliding guide block, and the other end is fixed to the wall. The sliding block is connected to the driver's seat via a hard bar with length d, the two joints of the hard bar can freely rotate, and the hard bar is joined in the horizontal direction by an angle θ. The model of the TDSS added by the NSE is plotted in Fig. 1(a). a is the distance in the horizontal direction between the seat and wall, b is the initial length of the horizontal spring, and e is the length of the horizontal spring after deformation. X_0 is the distance from the initial position of the driver's seat to the vehicle floor in the vertical direction; m is the driver's seat mass; c and k are the damping and stiffness coefficients of the TDSS, respectively; and F_{ns} and F are the force responses of the NSE and TDSS, respectively.

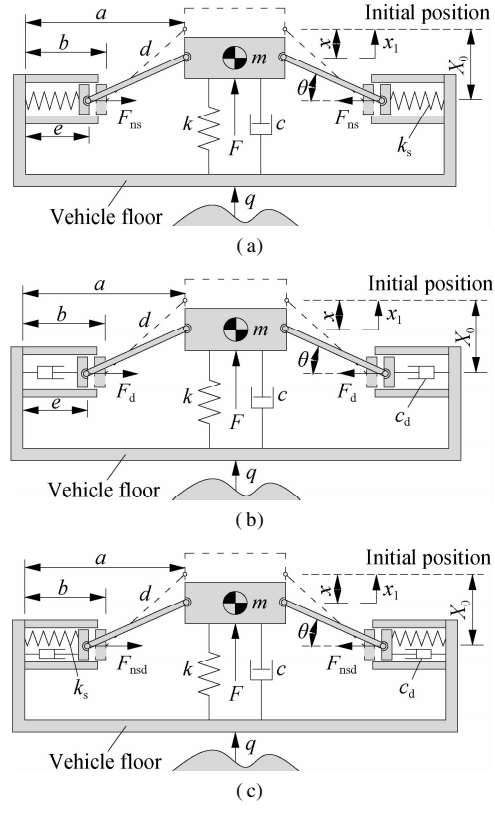

Fig. 1 Dynamic model of the TDSS. (a) Added by the NSE; (b) Added by the DE; (c) Added by the NSDE

To compute the force responses of F_{ns} and F, some assumptions are given as follows:

1) The sliding block and hard bar mass are negligible.

2) The friction generated at the joint of the hard bar and the sliding block is also negligible.

3) The vibration model of the TDSS equipped with the NSE is only evaluated in the vertical direction.

Under the load of $P = mg$ in Fig. 1(a), the driver's seat is then moved down a distance x from the initial position of X_0. The force response F of the TDSS added by the NSE is expressed as follows:

$$F = c\dot{x} + kx + F_{\mathrm{xs}} \tag{1}$$

where F_{xs} is the vertical restoring force generated by the compression force F_{ns} of two horizontal springs, and it is determined as follows:

$$\left.\begin{aligned} F_{\mathrm{xs}} &= 2k_s\left(1 - \frac{a-b}{\sqrt{d^2 - (X_0 - x)^2}}\right)(X_0 - x) \\ X_0 &= \sqrt{d^2 - (a-b)^2} \end{aligned}\right\} \tag{2}$$

Thus, the force F in Eq. (1) is rewritten by

$$F = c\dot{x} + kx + 2k_s\left(1 - \frac{a-b}{\sqrt{d^2 - (X_0 - x)^2}}\right)(X_0 - x) \tag{3}$$

1.1.2 Model of the DE added in the TDSS

Based on the structure model of the NSE in Fig. 1(a), two springs of the NSE were replaced using two dampers with the damping parameter c_d, as provided in Fig. 1(b). F_d and F are the force responses of the DE and TDSS, respectively.

Similarly, the deformation of the seat generated under the effect of the load of $P = mg$ is defined by x. Thus, the TDSS's force response added by the DE is calculated as

$$F = c\dot{x} + kx + F_{xd} \tag{4}$$

where F_{xd} is the vertical damping force generated by two horizontal dampers, and it is determined as

$$\left.\begin{aligned} F_{xd} &= 2F_d\tan\theta = 2c_d(\dot{b} - \dot{e})\frac{X_0 - x}{a - e} \\ e &= a - \sqrt{d^2 - (X_0 - x)^2} \end{aligned}\right\} \tag{5}$$

Due to the parameter of b being constant, $\dot{b} = 0$. The damper's displacement speed is calculated by

$$\dot{e} = \frac{\mathrm{d}}{\mathrm{d}t}\left(a - \sqrt{d^2 - (X_0 - x)^2}\right) = \frac{-(X_0 - x)}{\sqrt{d^2 - (X_0 - x)^2}} \tag{6}$$

By substituting Eq. (6) into Eq. (5) and transforming Eq. (5), we have

$$F_{xd} = 2c_d\frac{(X_0 - x)^2}{d^2 - (X_0 - x)^2} \tag{7}$$

Thus, the force F in Eq. (4) is also rewritten as

$$F = c\dot{x} + kx + 2c_d\frac{(X_0 - x)^2}{d^2 - (X_0 - x)^2} \tag{8}$$

1.1.3 Combination model of the NSE and DE added in the TDSS

From the NSE and DE models in Figs. 1(a) and 1(b), the horizontal springs of the NSE and the horizontal dampers of the DE were combined and added in the TDSS, as shown in Fig. 1(c), where F_{nsd} is the force response of the NSDE.

The force response F of the TDSS added by the NSDE is also expressed as

$$F = c\dot{x} + kx + F_{xsd} \tag{9}$$

F_{xsd} is the vertical force generated by the horizontal dampers and springs. F_{xsd} is determined as follows:

$$\left.\begin{aligned} F_{xsd} &= 2c_d\frac{(X_0 - x)^2}{X^2} + 2k_s\left(1 - \frac{a - b}{X}\right)(X_0 - x) \\ X &= \sqrt{d^2 - (X_0 - x)^2} \end{aligned}\right\} \tag{10}$$

Based on the dynamic models of the driver's seat suspension system with the NSE, DE, and NSDE in Figs. 1(a) to (c), it is assumed that the vertical vibration q from the vehicle floor is transmitted to the driver's seat. The driver's seat vibration generated under the excitation q is defined by x_1, as described in Figs. 1(a) to (c). The vibration equation of the driver's seat is then expressed as

$$m\ddot{x}_1 = c(\dot{q} - \dot{x}_1) + k(q - x_1) + 2F_x \tag{11}$$

where F_x is the force response of the NSE, DE, and NSDE determined in Eqs. (2), (7), and (10), respectively, and F_x is rewritten as

$$F_x = \begin{cases} k_s\left(1 - \dfrac{a - b}{X}\right)(X_0 - x) & \text{with NSE} \\ c_d\dfrac{(X_0 - x)^2}{X^2} & \text{with DE} \\ c_d\dfrac{(X_0 - x)^2}{X^2} + k_s\left(1 - \dfrac{a - b}{X}\right)(X_0 - x) & \text{with NSDE} \end{cases} \tag{12}$$

With $\alpha_1 = d/b$, $\alpha_2 = a/b$, $\beta_1 = k_s/k$, and $\beta_2 = c_d/c$, Eq. (12) can be rewritten as

$$F_x = \begin{cases} \beta_1 k\left(1 - \dfrac{\alpha_2 - 1}{\bar{X}}\right)(X_0 - x) & \text{with NSE} \\ \beta_2 c\dfrac{(X_0 - x)^2}{\bar{X}^2} & \text{with DE} \\ \beta_2 c\dfrac{(X_0 - x)^2}{\bar{X}^2} + \beta_1 k\left(1 - \dfrac{\alpha_2 - 1}{\bar{X}}\right)(X_0 - x) & \text{with NSDE} \end{cases} \tag{13}$$

where $X_0 - x = x_1 - q$; $\bar{X} = \sqrt{\alpha_1^2 - (X_0 - x)^2/b^2}$; α_1 and α_2 are the geometrical dimension ratios of the NSE, DE, and NSDE; and β_1 and β_2 are the stiffness ratio and damping ratio of the NSE, DE, and NSDE, respectively.

Therefore, Eqs. (11) and (13) are used to assess the isolation performance of the NSE, DE, and NSDE and the effect of their dynamic parameters on ameliorating the driver's ride comfort.

1.2 Vibration excitations

In the moving condition of vehicles, the vibrations from the vehicle floor transmitted to the driver's seat suspension are mainly generated by two different excitation sources, namely, one random excitation of the road surface roughness and another excitation of the combined harmonics generated by the transmission, engine, and main/tail rotor connected together. Two excitation sources are described as follows.

1.2.1 Random excitation

To evaluate the performance of the NSE, DE, and NSDE in improving the driver's ride comfort, the random excitation from the vehicle floor built based on the power spectrum density (PSD) $S(n_0)$ in the ISO 8068 standard[19] was then applied. The PSD $S(f)$ of the random excitation from the vehicle floor in the frequency region is written as[6]

$$S(f) = S(n_0)\left(\frac{n}{n_0}\right)^{-2}v^{-1} = S(n_0)n_0^2vf^{-2} \tag{14}$$

where v is the speed; $n_0 = 0.1$ is the reference spatial frequency; $n = f/v$ is the spatial frequency; and f is the random excitation frequencies.

Based on the random signal of the white noise W and PSD $S(f)$ in Eq. (14), the random excitation of the floor in the time region is written as[4]

$$\dot{q} + 2\pi n_0 v^2 q = 2\pi n_0 \sqrt{S(f)v}\,W \tag{15}$$

The existing studies showed that the random excitation in the low-frequency region greatly affects the driver's ride comfort and health[18,20], especially excitation frequencies below 10 Hz. Thus, based on a value of $S(n_0) = 64 \times 10^{-6}$ m^3 of ISO level B in ISO 8068[19], $f \leqslant 10$ Hz, and $v = 20$ m/s, these parameters were then applied to compute the random excitation q of the vehicle floor. The simulation result is plotted in Fig. 2(a).

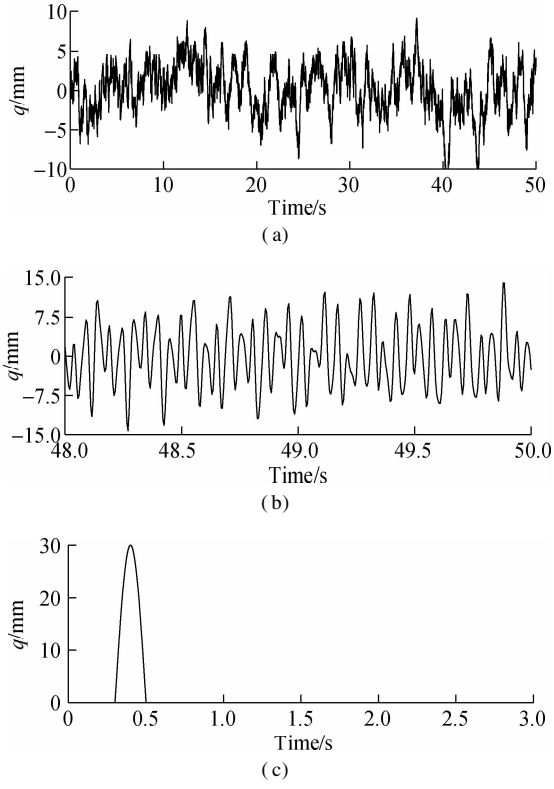

Fig. 2 Vibration excitations. (a) Random excitation; (b) Combined harmonic excitation; (c) Bumpy excitation

1.2.2 Combined harmonic excitation

The vibration excitations of the engine, transmission, and main/tail rotor connected together also affect the driver's ride comfort. In particular, the different excitation frequencies of the main rotor ($f_1 = 5.2$ Hz), tail rotor ($f_2 = 12.7$ Hz), hydraulic pump ($f_3 = 19.5$ Hz), rotor drive shaft ($f_4 = 25.3$ Hz), transmission input shaft ($f_5 = 32.6$ Hz), and oil cooler ($f_6 = 41.7$ Hz) are greatly affected the human body health[21]. Accordingly, the excitation of these multi-frequency wave harmonics is described as

$$q = \sum_{i=1}^{6} Q_i \sin(2\pi f_i t) \tag{16}$$

where Q_i and f_i are the amplitude vibrations and excitation frequencies of the rotating mechanisms, respectively, and $i = 1, 2, \ldots, 6$.

Based on the parameters of Q_i and f_i provided in Tab. 1[21], the combined harmonic excitation is then simulated and plotted in Fig. 2(b).

Tab. 1 Vibration excitation of rotating mechanisms

i	1	2	3	4	5	6
f_i/Hz	5.2	12.7	19.5	25.3	32.6	41.7
Q_i/mm	5.2	6.5	13.6	1.7	4.1	4.3

1.2.3 Bumpy excitation

The bumpy excitation from the vehicle floor could generate the maximum values of the seat acceleration and seat suspension's deformation in a very short time. It can also affect the driver's ride comfort and the durability of the driver's seat suspension. The mathematical equation of the bumpy excitation is expressed as

$$q = \begin{cases} 0 & \text{else} \\ 0.03\cos(\omega t + 0.5\pi) & 0.3 \leqslant t \leqslant 0.5 \end{cases} \tag{17}$$

where $\omega = 2\pi v/L$, v is the vehicle velocity, and L is the bump width. It is assumed that the vehicle is moving at a velocity of $v = 5$ m/s on $L = 0.4$ m. The bumpy excitation q was then simulated, as shown in Fig. 2(c).

The vibration excitations in Fig. 2 were then applied to evaluate the performance of the NSE, DE, and NSDE.

2 Influence of Design Parameters on the Performance of the Driver's Seat Suspension

2.1 Evaluation index

The performance of the vehicle's suspension system was assessed using some indexes, such as the ride comfort, road friendliness, and deformation of the suspension system[1-2,6,18]. The deformation of the driver's seat suspension system was evaluated via the weighted RMS deformation (x_{RMS}), and the driver's ride comfort was reflected via the weighted RMS acceleration of the driver's seat (a_{RMS})[6,18]. Both of these values are written as

$$\left.\begin{aligned} x_{\mathrm{RMS}} &= \sqrt{\frac{1}{T}\int_0^T (x_1 - q)^2 \mathrm{d}t} \\ a_{\mathrm{RMS}} &= \sqrt{\frac{1}{T}\int_0^T (\ddot{x}_1)^2 \mathrm{d}t} \end{aligned}\right\} \tag{18}$$

where x_1 and $\ddot{x}_1$ are calculated from Eq. (11) in the simulation time T.

To evaluate the performance of the NSE, DE, and NSDE on isolating the driver's ride comfort, the decreases in x_{RMS} and a_{RMS} are chosen as the evaluation indexes.

2.2 Sensitivity analysis of design parameters

The change in the design parameters of the suspension

system affects the ride comfort[10, 15, 17]. Thus, to analyze the sensitivity of the NSE, DE, and NSDE parameters on the driver's ride comfort, the initial parameters of the driver's seat suspension, ratios of the geometrical dimensions α_1 and α_2, stiffness ratio β_1, and damping ratio β_2 provided in Tab. 2[10, 17] were simulated.

Tab. 2 Design parameters of the driver's seat suspension with the NSE, DE, and NSDE

Parameters	Values	Parameters	Values
m/kg	85	k/(kN · m^{-1})	40
b/mm	230	c/(kN · s · m^{-1})	0.35
α_1	0.78	β_1	0.65
α_2	1.20	β_2	0.65

Under the random excitation of the vehicle floor on the driver's seat suspension presented in Fig. 2(a), the influence of the geometrical dimension ratios of the NSE, DE, and NSDE, including $\alpha_1 = d/b = \{0.5, 0.6, \ldots, 1.4\}$ and $\alpha_2 = a/b = \{1.0, 1.1, \ldots, 2.0\}$ on x_{RMS} and a_{RMS}, were computed and are plotted in Fig. 3(a) to (c), respectively.

With the driver's seat suspension added by the NSE, Fig. 3(a) shows that x_{RMS} and a_{RMS} are strongly affected by the changes in α_1 and α_2. x_{RMS} can obtain the minimum value when $0.7 \leqslant \alpha_1 \leqslant 1.2$ and $1.0 \leqslant \alpha_2 \leqslant 1.4$, whereas a_{RMS} can obtain the minimum value when $0.8 \leqslant \alpha_1 \leqslant 1.4$ and $1.1 \leqslant \alpha_2 \leqslant 1.5$. To reach the minimum x_{RMS} and a_{RMS}, the ratios of α_1 and α_2 should be optimized at a range of $0.8 \leqslant \alpha_1 \leqslant 1.2$ and $1.1 \leqslant \alpha_2 \leqslant 1.4$.

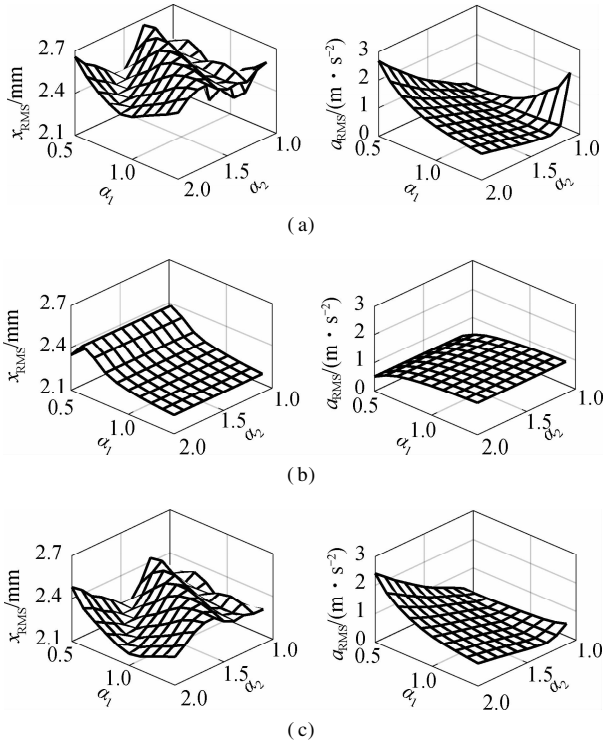

Fig. 3 Influence of the geometrical dimension ratios on x_{RMS} and a_{RMS}. (a) With NSE; (b) With DE; (c) With NSDE

With the driver's seat suspension added by the DE, Fig. 3(b) shows that x_{RMS} and a_{RMS} are significantly influenced by α_1, but they are not affected by α_2. This result can be due to the force F_{xd} of the DE in Eq. (7) not being affected by the ratio of $\alpha_2 = a/b$. In addition, x_{RMS} increased and a_{RMS} decreased with the increase in α_1 and vice versa. Thus, to obtain the minimum x_{RMS} and a_{RMS}, the ratio of α_1 should be optimized at a range of $0.8 \leqslant \alpha_1 \leqslant 1.2$.

With the driver's seat suspension added by the NSDE, similar to the results of the NSE, Fig. 3(c) shows that x_{RMS} and a_{RMS} are also strongly influenced by the changes in α_1 and α_2. This result can be due to the effect of the geometrical dimension ratios of the NSE in the NSDE. At ranges of $0.7 \leqslant \alpha_1 \leqslant 1.4$ and $1.0 \leqslant \alpha_2 \leqslant 1.5$, x_{RMS} and a_{RMS} can achieve the minimum value. Thus, α_1 and α_2 should also be selected in this region to optimize the results of x_{RMS} and a_{RMS}.

Similarly, under the random excitation of the vehicle floor in Fig. 2(a), the change in the stiffness and damping parameters ($\delta_1 k$ and $\delta_2 c$) and the stiffness and damping ratios (β_1 and β_2) of the NSE, DE, and NSDE on x_{RMS} and a_{RMS} were also computed and are shown in Figs. 4(a) to (c), respectively. $\delta_{1,2} = \{0.2, 0.4, \ldots, 2.0\}$ and $\beta_{1,2} = \{0.1, 0.2, \ldots, 1.0\}$.

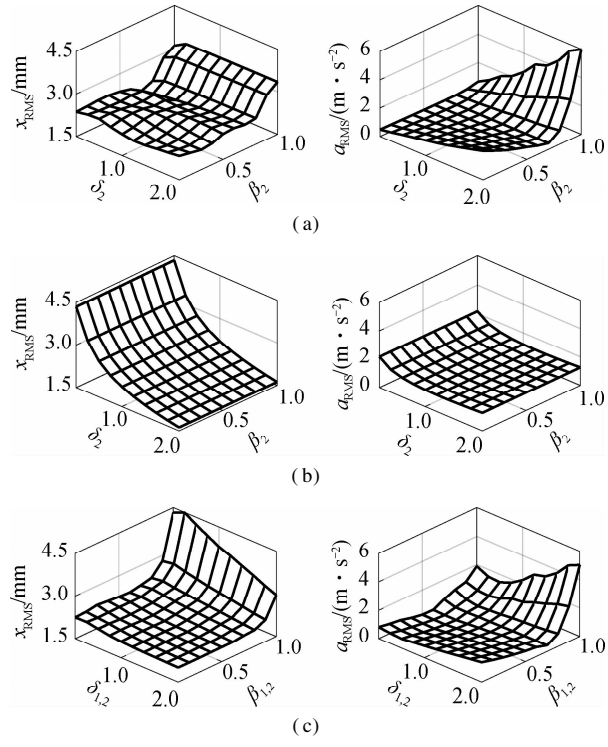

Fig. 4 Influence of the ratios of the dynamic stiffness and damping parameters on x_{RMS} and a_{RMS}. (a) With NSE; (b) With DE; (c) With NSDE

With the NSE, Fig. 4(a) indicates that x_{RMS} and a_{RMS} are strongly affected by the change in δ_1 and β_1. At a range of $0.5 \leqslant \beta_1 \leqslant 0.75$ and $0.5 \leqslant \delta_1 \leqslant 1.0$, x_{RMS} and

a_{RMS} can obtain the minimum value. Therefore, the range of δ_1 and β_1 should also be selected to optimize the results of x_{RMS} and a_{RMS}.

With the DE, Fig. 4(b) also shows that x_{RMS} and a_{RMS} are remarkably affected by δ_2, but they are insignificantly affected by β_2. This finding implies that the change in the damping coefficient c_{d} of the DE insignificantly affects x_{RMS} and a_{RMS}. Here the change in x_{RMS} and a_{RMS} is mainly due to the change in the damping coefficient c of the TDSS. x_{RMS} and a_{RMS} increased when the damping coefficient c was reduced and vice versa. To obtain the minimum value of x_{RMS} and a_{RMS}, a range of $0.6 \leqslant \delta_2 \leqslant 1.5$ should be optimized.

With the NSDE, Fig. 4(c) indicates that x_{RMS} and a_{RMS} are affected by the stiffness k and stiffness ratio $\beta_1 = k_{\mathrm{s}}/k$ of the NSE and the damping coefficient c of the TDSS. To reduce x_{RMS} and a_{RMS}, a range of $0.6 \leqslant \delta_{1,2} \leqslant 1.5$ and $0.5 \leqslant \beta_{1,2} \leqslant 0.75$ should be used.

Based on the above analysis results, the change in the design parameters of the NSE, DE, and NSDE remarkably affect the driver's ride comfort. However, it is difficult to fully evaluate the performance of the NSE, DE, and NSDE based on their initial design parameters because the parameters in each model of the NSE, DE, and NSDE changed could also affect the results of x_{RMS} and a_{RMS}. Accordingly, all design parameters of each model need to be optimized. Then, the optimization results are used to evaluate the performance of the NSE, DE, and NSDE in the driver's seat suspension system.

2.3 Optimizing NSE, DE, and NSDE parameters

To optimize the NSE, DE, and NSDE parameters, the boundary conditions need to be defined. Based on the analysis results in Section 2.2, the boundary conditions of the NSE, DE, and NSDE parameters are defined as

$$\begin{aligned} d &= \alpha_1 b \qquad 0.8 \leqslant \alpha_1 \leqslant 1.2 \\ a &= \alpha_2 b \qquad 1.1 \leqslant \alpha_2 \leqslant 1.4 \\ b &= 230 \text{ mm} \\ k_{\mathrm{s}} &= \beta_1 k \qquad 0.5 \leqslant \beta_1 \leqslant 0.75 \\ k &= 40\delta_1 \text{ kN/m} \qquad 0.5 \leqslant \delta_1 \leqslant 1.0 \\ c_{\mathrm{d}} &= \beta_2 c \qquad 0.5 \leqslant \beta_2 \leqslant 0.75 \\ c &= 350\delta_2 \text{ N} \cdot \text{s/m} \qquad 0.6 \leqslant \delta_2 \leqslant 1.5 \end{aligned} \tag{19}$$

Based on the boundary conditions in Eq. (19), the design parameters of the NSE, DE, and NSDE need to be optimized to obtain the minimum x_{RMS} and a_{RMS}. Thus, the objective functions of the NSE, DE, and NSDE are expressed as

$$\left.\begin{aligned} G &= \min\{x_{\mathrm{RMS}}, a_{\mathrm{RMS}}\} \\ x_{\mathrm{RMS}} &= \left(T^{-1}\int_0^T (x_1 - q)^2 \mathrm{d}t\right)^{1/2} \\ a_{\mathrm{RMS}} &= \left(T^{-1}\int_0^T \ddot{x}_1^2 \mathrm{d}t\right)^{1/2} \end{aligned}\right\} \tag{20}$$

Eqs. (19) and (20) indicate that this is a multi-objective optimization problem. Thus, to solve this issue, a multi-objective optimization method using the GA[5, 14, 20] was applied to optimize the object function G of the NSE, DE, and NSDE.

The GA is defined as finding a vector of $\boldsymbol{x} = \{x_1, x_2, \ldots, x_n\}^{\mathrm{T}}$ satisfying the initial conditions to achieve the minimum or maximum values of $\boldsymbol{G}(\boldsymbol{x}) = \{g_1(x), g_2(x), \ldots, g_n(x)\}^{\mathrm{T}}$. The structure of the GA is defined by the processes of encoding, population initialization, fitness evaluation, parent selection, genetic operations (crossover and mutate), and termination criterion[4-5]. The GA has been used for optimizing the NSE, DE, and NSDE parameters as follows:

Based on the dynamic model of the driver's seat in Fig. 1 and the boundary conditions in Eq. (19), the GA was applied to search a vector of $\boldsymbol{x} = \{\alpha_1, \alpha_2, \delta_1, \delta_2, \beta_1, \beta_2\}^{\mathrm{T}}$ of the NSE, DE, and NSDE models to achieve the minimum value of $\boldsymbol{G} = \{x_{\mathrm{RMS}}, a_{\mathrm{RMS}}\}^{\mathrm{T}}$. The structure flowchart and setting parameters of the optimization model are plotted in Fig. 5 and defined in Tab. 3, respectively.

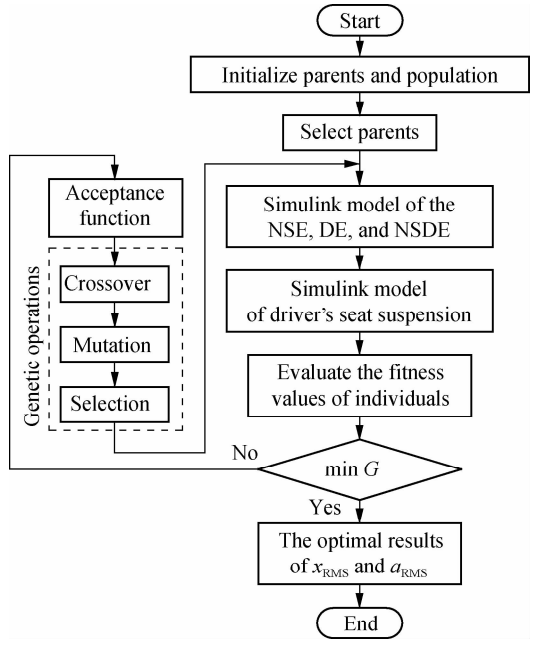

Fig. 5 Structure of the GA and seat suspension

Tab. 3 Initial parameters established in the GA

Parameter	Value	Parameter	Value
Generations	1 000	Crossover probability	0.95
Initial populations	150	Termination criterion of $\lvert G_i(x) - G_{i+1}(x) \rvert$	1.0×10^{-3}
Mutation probability	0.05		

Based on the random excitation of the vehicle floor in Fig. 2(a) and the GA's operation parameters in Tab. 3, the design parameters of the NSE, DE, and NSDE are then optimized via the algorithm flowchart in Fig. 5 to obtain the minimum value of $\boldsymbol{G} = \{x_{\mathrm{RMS}}, a_{\mathrm{RMS}}\}^{\mathrm{T}}$. The optimal results of the NSE, DE, and NSDE are shown in Fig. 6. The results show that the distribution densities of

x_{RMS} and a_{RMS} with the NSE, DE, and NSDE decremented in the optimization process. The minimum values of $\boldsymbol{G} = \{x_{RMS}, a_{RMS}\}^T$ with the NSE, DE, and NSDE optimized by the GA were achieved at $\{1.985, 0.428\}^T$, $\{1.558, 0.931\}^T$, and $\{1.470, 0.441\}^T$, respectively. At the minimum G, all the optimal parameters were saved and are provided in Tab. 4. Moreover, the change in the design parameters before and after optimization are listed and compared in Tab. 5. The optimal parameters of each model were then simulated to assess the performance of the NSE, DE, and NSDE.

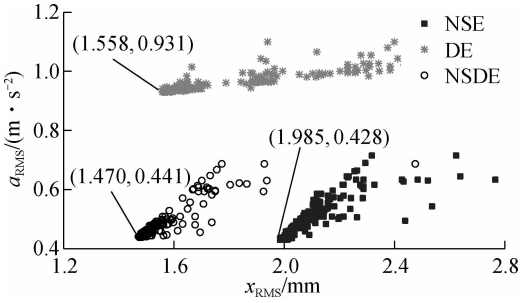

Fig. 6 Distribution densities of x_{RMS} and a_{RMS}

Tab. 4 Optimal results of the NSE, DE, and NSDE

Parameters	NSE	DE	NSDE
α_1	0.901	0.823	0.960
α_2	1.152	1.152	1.151
δ_1	0.880	1.000	0.901
δ_2	1.000	1.340	1.321
β_1	0.600	1.000	0.591
β_2	1.000	0.610	0.590

Tab. 5 Optimized dynamic parameters

Isolations	Parameters	Before optimization	After optimization	Change value/%
With NSE	a/mm	276.0	265.0	−4.15
	d/mm	179.4	207.2	13.42
	k_s/(kN · m^{-1})	26.0	21.1	−23.22
	k/(kN · m^{-1})	40.0	35.2	−13.64
With DE	a/mm	276.0	276.0	0.00
	d/mm	179.4	189.3	5.23
	c_d/(kN · s · m^{-1})	0.23	0.29	20.69
	c/(kN · s · m^{-1})	0.35	0.47	25.53
With NSDE	a/mm	276.0	264.7	−4.27
	d/mm	179.4	220.8	18.75
	k_s/(kN · m^{-1})	26.0	21.3	−22.07
	k/(kN · m^{-1})	40.0	36.0	−11.11
	c_d/(kN · s · m^{-1})	0.23	0.25	8.00
	c/(kN · s · m^{-1})	0.35	0.43	18.60

2.3.1 Performance of the NSE, DE, and NSDE under a random excitation

Under the moving condition of the vehicle on the road surface roughness, the random excitation of the vehicle floor in Fig. 2(a) was used to the isolation performance of the optimized NSE, DE, and NSDE. The simulation results of the driver's seat suspension deformation and driver's seat acceleration responses are plotted in Figs. 7(a) and 7(b).

Fig. 7 shows that the driver's seat suspension deformation and acceleration responses with the DE significantly reduced as compared to the TDSS, whereas the driver's seat suspension deformation and acceleration responses with the NSE and NSDE strongly decreased in comparison with the TDSS, especially with the NSDE. Moreover, the RMS results of the seat suspension deformation and seat acceleration were calculated and are provided in Tab. 6.

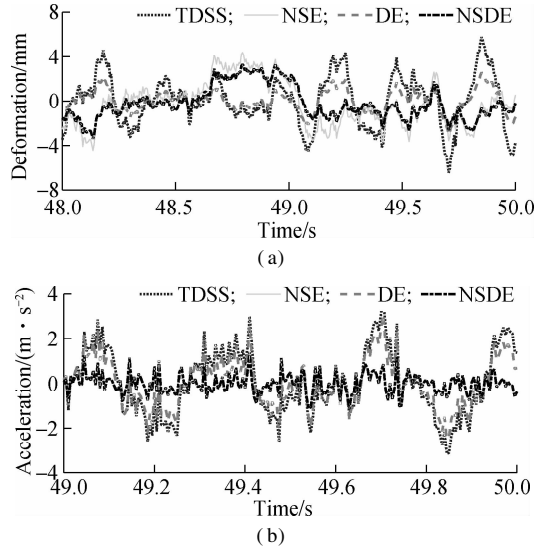

Fig. 7 Simulation results under random excitation. (a) Suspension deformation; (b) Seat acceleration

Tab. 6 Calculation results of x_{RMS} and a_{RMS}

Parameters	x_{RMS}/mm	a_{RMS}/(m · s^{-2})
TDSS	2.202 6	1.188 8
NSE	1.963 3	0.421 5
DE	1.548 3	0.932 4
NSDE	1.479 0	0.445 4

With the NSE, x_{RMS} and a_{RMS} remarkably reduced by 10.86% and 64.54% in comparison with those with the TDSS, especially the driver's seat RMS acceleration. This finding implies that the seat suspension deformation and driver's ride comfort are better than those of the TDSS. This result is attributed to the restoring force of the NSE generated to reduce the force response of the driver's seat suspension (see Fig. 8(a)), and the NSE has an obvious effect on improving the driver's ride quality. This result is also similar to those of existing studies[10−11, 14, 17].

With the DE, x_{RMS} was significantly reduced by 29.71%, while a_{RMS} was slightly reduced by 21.57% compared to the TDSS. Hence, the TDSS added by the DE is only effective in improving the seat suspension deformation. In addition, the analysis results of the DE in Figs. 3(b) and 4(b) show that x_{RMS} and a_{RMS} are insignificantly affected by the geometrical dimension ratio and da-

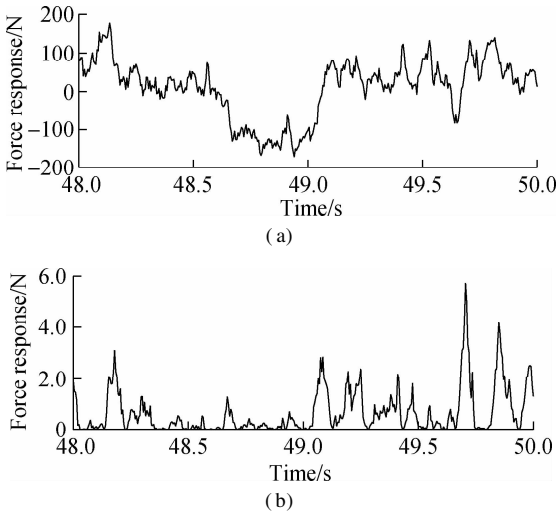

Fig. 8 Force response of the seat suspension under the random excitation. (a) With NSE (RMS of F_{xs} is 62.8 N); (b) With DE (RMS of F_{xd} is 1.06 N)

mping ratio of the DE. Moreover, the simulation result of the damping force F_{xd} of the DE in Fig. 8(b) shows that the damping force response of the DE is very small in comparison with the restoring force response of the NSE (RMS of F_{xd} is less than the RMS of F_{xs} by 98.3%). This result is due to the value of $(X_0 - x)^2$ of the DE in Eq. (7) being very small, so the damping force response of the DE obtained is also very small. Hence, the DE is not effective in improving the driver's ride comfort and seat suspension deformation. The small results of the seat suspension deformation and driver's seat acceleration and x_{RMS} and a_{RMS} of the DE compared to the TDSS in Figs. 7 and 8 are due to the optimized damping coefficient c of the TDSS being increased by 25.53% (see Tab. 5). Therefore, the DE was not studied and applied to the TDSS. However, this issue is hardly mentioned in the existing studies.

With the NSDE, the calculation results in Fig. 7(a) and Tab. 6 show that the seat suspension deformation and its x_{RMS} are the smallest. x_{RMS} is greatly reduced by 32.85% compared to the TDSS. This is due to the damping coefficient c being increased by 18.60% and the stiffness coefficient of k being reduced by 11.11% after the optimization process (see Tab. 5). Moreover, a_{RMS} value strongly decreased by 62.53% in comparison with the TDSS, and a_{RMS} of the NSDE was only 5.4% higher than the NSE. This result is attributed to the performance of the optimized NSE.

Based on the above analysis results, the DE is not effective in improving the driver's ride comfort and seat suspension deformation, whereas the NSE has an obvious effect on improving the driver's ride quality. To improve the seat suspension deformation and acceleration of the driver's seat, the NSE and optimized damping coefficient c should be used on the TDSS.

2.3.2 Performance of the NSE, DE, and NSDE under the combined harmonic excitation

To further evaluate the isolation performance of the NSE, DE, and NSDE, a combined harmonic excitation of the engine, transmission, and main/tail rotor transmitted to the vehicle floor in Fig. 2(b) was used for the simulation process. The seat suspension deformation and driver's seat acceleration are plotted in Figs. 9(a) and (b).

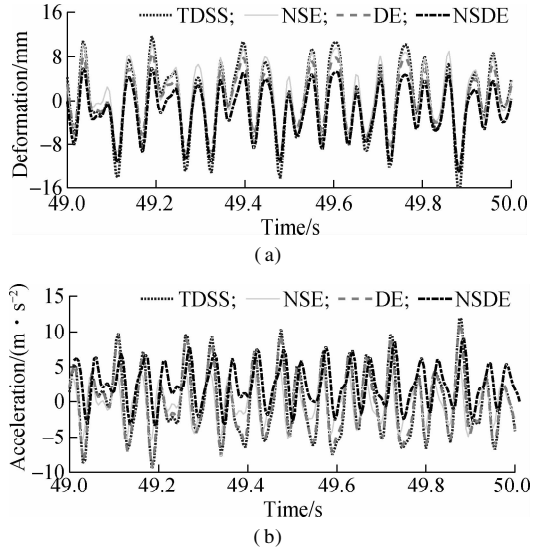

Fig. 9 Simulation results under the combined harmonic excitation. (a) Suspension deformation; (b) Seat acceleration

Similarly, Fig. 9(a) shows that the seat suspension deformation with the DE is lower than that of the NSE, and the seat suspension deformation with the NSDE is the smallest. Conversely, the driver's seat acceleration with the DE is insignificantly reduced compared to that with the TDSS, whereas it is greatly decreased by the NSE and NSDE (see Fig. 9(b)). Based on the simulation data in Fig. 9, x_{RMS} and a_{RMS} of the TDSS, NSE, DE, and NSDE were also computed and are listed in Tab. 7.

Tab. 7 Calculation results of x_{RMS} and a_{RMS}

Parameters	x_{RMS}/mm	a_{RMS}/(m · s^{-2})
TDSS	6.656 2	4.827 7
NSE	6.095 4	2.820 4
DE	5.310 2	4.512 2
NSDE	5.012 2	2.985 4

The results also show that x_{RMS} and a_{RMS} of the NSE are lower than those of the TDSS by 8.43% and 41.58%, respectively. In particular, the a_{RMS} value of the NSE is strongly reduced compared to the TDSS. This is also due to the influence of the restoring force generated by the optimized NSE, as plotted in Fig. 10(a). On the contrary, due to the very small damping force generated by the DE in Fig. 10(b), a_{RMS} of the DE in Tab. 7 is only reduced by 6.54% compared to the TDSS, and a_{RMS} of the DE is higher than that of the NSE by 37.5%. x_{RMS} with the DE

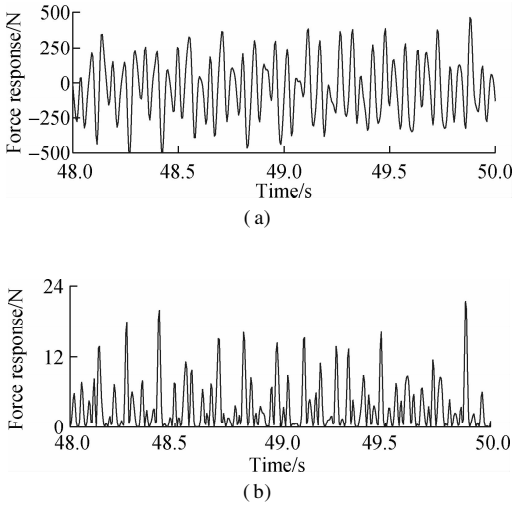

Fig. 10 Force response of the seat suspension under the combined harmonic excitations. (a) With NSE (RMS of F_{xs} is 216.4 N); (b) With DE (RMS of F_{xd} is 5.38 N)

reduced by 20.22% in comparison with the TDSS in Tab. 7, which is mainly due to the optimized damping coefficient c. Therefore, the DE is ineffective under the combined harmonic excitation.

With the NSDE used by the optimal damping coefficient c of the TDSS and optimal NSE combined, its x_{RMS} decreased by 24.70% in comparison with the TDSS, and its value is also the lowest. Moreover, its a_{RMS} value strongly decreased by 38.16% in comparison with the TDSS, and it is only higher than the NSE by 5.5%. This result implies that the DE should be ignored, and the optimal damping coefficient c of the TDSS and optimal NSE should be combined to further improve the seat suspension deformation and driver's ride comfort under the combined harmonic excitation.

2.3.3 Performance of the NSE, DE, and NSDE under the bumpy excitation

The isolation performance of the NSE, DE, and NSDEwas also evaluated under the bumpy excitation of the vehicle floor in Fig. 2(c). The simulation results of the seat suspension deformation and driver's seat acceleration are plotted in Figs. 11(a) and 11(b).

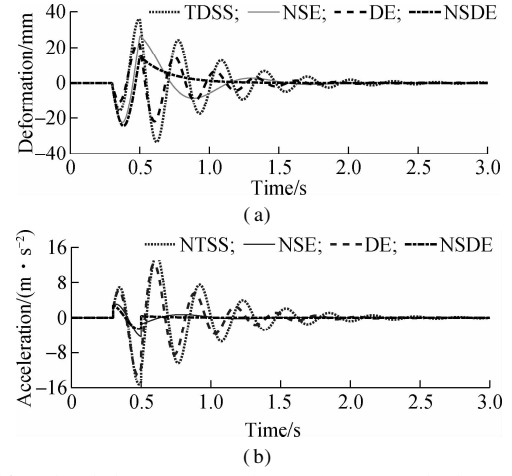

Fig. 11 Simulation results under the bumpy excitation. (a) Suspension deformation; (b) Seat acceleration

Similarly, Fig. 11(a) shows that the seat suspension deformation with the DE is lower than that of the NSE, and the seat suspension deformation with the NSDE is the smallest. Conversely, Fig. 11(b) indicates that the seat acceleration with the DE is slightly decreased compared to the TDSS, whereas it is greatly decreased by the NSE and NSDE. Hence, the DE is also ineffective under the bumpy excitation. Therefore, the DE should also be ignored, and the optimal damping coefficient c of the TDSS and optimal NSE should be applied to improve the driver's ride comfort under the bumpy excitation.

3 Conclusions

1) The sensitivity of the geometric dimension ratios (α_1 and α_2), stiffness parameter (k), and stiffness ratio (β_1) of the NSE and NSDE greatly affect the seat suspension deformation and driver's seat acceleration. Conversely, the DE's design parameters insignificantly affect the seat suspension deformation and driver's seat acceleration.

2) With the design parameters of the NSE, DE, and NSDE optimized under the random excitation of the vehicle floor, the research result shows that the damping force generated by the DE is very small in comparison with the restoring force generated by the NSE under random excitation and combined harmonic excitation. Therefore, the DE added in the TDSS is not effective in reducing the seat suspension deformation and improving the driver's ride comfort.

3) The NSE added into the TDSS greatly improves the ride comfort of the driver's seat. However, the NSE insignificantly improves the seat suspension deformation. To improve the driver's ride comfort and seat suspension deformation, the TDSS should be added by the NSE, whereas the damping coefficient c of the TDSS should be optimized or controlled. This is also the reason why the NSE was studied and added in TDSS, while the damping coefficient c of the TDSS was also independently controlled in the existing studies. However, combining the NSE and controlled damping coefficient for the TDSS has not been considered. Thus, this issue needs to be further studied in future works.

References

[1] Hostens I, Deprez K, Ramon H. An improved design of air suspension for seats of mobile agricultural machines[J]. *Journal of Sound and Vibration*, 2004, **276**(1/2): 141 − 156. DOI: 10.1016/j.jsv.2003.07.018.

[2] Maciejewski I. Control system design of active seat suspensions[J]. *Journal of Sound and Vibration*, 2012, **331**(6): 1291 − 1309. DOI: 10.1016/j.jsv.2011.11.010.

[3] Liu J, Xu Z, Shao Y, et al. An optimization design method for a body mounting system of a heavy vehicle [J]. *Journal of Materials*: *Design and Applications*, 2017, **233**: 1352 − 1362, DOI: 10.1177/1464420717748971.

[4] Wang W, Song Y L, Xue Y B, et al. An optimal vibration control strategy for a vehicle's active suspension based on improved cultural algorithm[J]. *Applied Soft Computing*,

2015, **28**: 167 − 174. DOI: 10. 1016/j. asoc. 2014. 11. 047.
[5] Nariman-Zadeh N, Salehpour M, Jamali A, et al. Pareto optimization of a five-degree of freedom vehicle vibration model using a MUGA [J]. *Engineering Applications of Artificial Intelligence*, 2010, **23**: 543 − 551. DOI: 10. 1016/j. engappai. 2009. 08. 008.
[6] Nguyen V, Jiao R Q, Zhang J R. Control performance of damping and air spring of heavy truck air suspension system with optimal fuzzy control [J]. *SAE International Journal of Vehicle Dynamic, Stability, and NVH*, 2020, **4**: 179 − 194. DOI: 10. 4271/10-04-02-0013.
[7] Yuan H, Nguyen V L, Zhou H X. Research on semi-active air suspensions of heavy trucks based on a combination of machine learning and optimal fuzzy control [J]. *SAE International Journal of Vehicle Dynamic*, *Stability*, *and NVH*, 2021, **5**: 159 − 172. DOI: 10. 4271/10-05-02-0011.
[8] Palomares E, Nieto A J, Morales A L, et al. Numerical and experimental analysis of a vibration isolator equipped with a negative stiffness system[J]. *Journal of Sound and Vibration*, 2018, **414**: 31 − 42. DOI: 10. 1016/j. jsv. 2017. 11. 006.
[9] Davoodi E, Safarpour P, Pourgholi M, et al. Design and evaluation of vibration reducing seat suspension based on negative stiffness structure [J]. *Part C*: *Journal of Mechanical Engineering Science*, 2020, **234**: 4171 − 4189, DOI: 10. 1177/0954406220921203.
[10] Zha J L, Nguyen V L, Su B B, et al. Performance of the seat suspension system using negative stiffness structure on improving the driver's ride comfort [J]. *International Journal of Vehicle Dynamic, Stability, and NVH*, 2022, **6**: 135 − 146. DOI: 10. 4271/10-06-02-0009.
[11] Li S H, Feng G Z, Zhao Q. Design and research of semiactive quasi-zero stiffness vibration isolation system for vehicles [J]. *Shock and Vibration*, 2021, **2021**: 1 − 22. DOI: 10. 1155/2021/5529509.
[12] Shi X, Zhu S Y. Simulation and optimization of magnetic negative stiffness dampers[J]. *Sensors and Actuators A*: *Physical*, 2017, **259**: 14 − 33. DOI: 10. 1016/j. sna. 2017. 03. 026.
[13] Zha J, Nguyen V, Ni D, et al. Optimizing the geometrical dimensions of the seat suspension equipped with a negative stiffness structure based on a genetic algorithm [J]. *SAE International Journal of Vehicle Dynamic, Stability, and NVH*, 2022, **6**: 147 − 158. DOI: 10. 4271/10-06-02-0010.
[14] Georgios P, Artemios V, Dimitrios K. Optimal design of passenger vehicle seat with the use of negative stiffness elements [J]. *Proc IMechE, Part D*: *J Automobile Engineering*, 2019, **234**: 610 − 629, DOI: 10. 1177/0954407019854879.
[15] Han J S, Meng L S, Sun J G. Design and characteristics analysis of a nonlinear isolator using a curved-mount-spring-roller mechanism as negative stiffness element [J]. *Mathematical Problems in Engineering*, 2018, **2018**: 1 − 15, DOI: 10. 1155/2018/1359461.
[16] Chen L, Wang J, Xu X, et al. Nonlinear analysis of a quasi-zero stiffness air suspension based on the cell-mapping method[J]. *The International Journal of Acoustics and Vibration*, 2021, **26** (2): 148 − 160. DOI: 10. 20855/ijav. 2021. 26. 21755.
[17] Le T D, Ahn K K. A vibration isolation system in low frequency excitation region using negative stiffness structure for vehicle seat[J]. *Journal of Sound and Vibration*, 2011, **330**(26): 6311 − 6335. DOI: 10. 1016/j. jsv. 2011. 07. 039.
[18] International Organization for Standardization. Mechanical vibration and shock-Evaluation of human exposure to whole body vibration-Part 2: General requirement: ISO 2631-1 [S]. Geneva, Switzerland: International Organization for Standardization, 1997.
[19] International Organization for Standardization. Mechanical vibration—Road surface profiles—Reporting of measured data: ISO 8068 [S]. Geneve, Switzerland: International Organization for Standardization, 1995.
[20] Nguyen V, Zhang J R, Le V Q, et al. Vibration analysis and modeling of an off-road vibratory roller equipped with three different cab's isolation mounts [J]. *Shock and Vibration*, 2018, **2018**: 1 − 17. DOI: 10. 1155/2018/8527574.
[21] Carletti E, Pedrielli F. Tri-axial evaluation of the vibration transmitted to the operators of crawler compact loaders [J]. *International Journal of Industrial Ergonomics*, 2018, **68**: 46 − 56. DOI: 10. 1016/j. ergon. 2018. 06. 007.

座椅悬架不同设计模式的隔振性能比较

查吉利[1,2] 张建润[3] 阮文廉[1,2]

([1] 湖北理工学院机电工程学院, 黄石 435003)
([2] 湖北理工学院智能输送技术与装备湖北重点实验室, 黄石 435003)
([3] 东南大学机械工程学院, 南京 211189)

摘要:为进一步改善车辆座椅乘坐舒适性,设计了 3 种分别基于负刚度结构单元(NSE)、阻尼结构单元(DE)及负刚度-阻尼单元(NSDE)的座椅悬架系统. 建立了座椅悬架动力学模型,以悬架位移幅和座椅加速度的均方根值为评价目标,考察了不同设计参数对座椅乘坐舒适性的影响特性,并利用遗传算法对悬架设计参数进行了优化分析. 研究结果表明:基于 NSE 和 DE 单元的悬架设计参数对评价目标的影响较大,通过参数优化分析发现 DE 的阻尼力比 NSE 的恢复力低 98. 3%,说明 DE 结构单元对改善座椅隔振性能作用有限. 但引入 NSE 结构单元后,NSDE 悬架系统的振动位移幅和座椅加速度的均方根值明显减小,有效提升了座椅的隔振效果,提高了驾驶员的乘坐舒适性.

关键词:座椅悬架;负刚度元件;阻尼元件;舒适性;遗传算法
中图分类号:U461. 3